Cerebral Cortex, August 2017;27: 4229–4243

doi: 10.1093/cercor/bhx124
Advance Access Publication Date: 19 May 2017
Original Article

ORIGINAL ARTICLE

Decomposing Tool-Action Observation: A Stereo-EEG Study

F. Caruana[1,2], P. Avanzini[1,2], R. Mai[3], V. Pelliccia[1,3], G. LoRusso[3], G. Rizzolatti[1,2] and G. A. Orban[1]

[1]Department of Neuroscience, University of Parma, Via Volturno 39, 43125 Parma, Italy, [2]CNR Institute of Neuroscience, Via Volturno 39, Parma, Italy and [3]Claudio Munari Center for Epilepsy Surgery, Ospedale Niguarda-Ca' Granda, 20162 Milan, Italy

Address correspondence to F. Caruana. Email: fausto.caruana@unipr.it

Abstract

A description of the spatiotemporal dynamics of human cortical activity during cognitive tasks is a fundamental goal of neuroscience. In the present study, we employed stereo-EEG in order to assess the neural activity during tool-action observation. We recorded from 49 epileptic patients (5502 leads) implanted with intracerebral electrodes, while they observed tool and hand actions. We deconstructed actions into 3 events—video onset, action onset, and tool-object contact—and assessed how different brain regions respond to these events. Video onset, with actions not yet visible, recruited only visual areas. Aligning the responses at action onset, yielded activity in the parietal-frontal manipulation circuit and, selectively for tool actions, in the left anterior supramarginal gyrus (aSMG). Finally, by aligning to the tool-object contact that signals the achievement of the main goal of the observed action, activations were found in SII and dorsal premotor cortex. In conclusion, our data show that during tool-action observation, in addition to the general action observation network there is a selective activation of aSMG, which exhibits internally different patterns of responsiveness. In addition, neural responses selective for the contact between the tool and the object were also observed.

Key words: gamma power, hand action observation, mirror system, stereo-EEG, tool-action observation

Introduction

A characteristic of *Homo sapiens* is his unique capacity to make and use tools. Humans have devised an incredible number of implements to enhance their motor repertoire, to reach further, to manipulate with more force, and to move faster. This capacity, together with imitation and language, has set our species apart from all other species of primates. A number of imaging studies have investigated tool use from the motor point of view using either actual tool actions (Johnson-Frey et al. 2005; Gallivan et al. 2013; Brandi et al. 2014), or tool use pantomime (Moll et al. 2000; Choi et al. 2001; Rumiati et al. 2004; Króliczak and Frey 2009; Chen et al. 2016), highlighting the role of the left inferior parietal lobe as a fundamental region for tool-action planning and execution. A large body of lesion studies in patients with ideomotor apraxia has also indicated the involvement of this region in tool use (Rothi et al. 1985; Ochipa et al. 1989; Goldenberg and Hagmann 1998; Buxbaum et al. 2000, 2005, 2014; Rumiati et al. 2001; Garcea et al. 2013; for review see De Renzi and Faglioni 1999; Goldenberg 2009; Osiurak et al. 2009; Heilman and Valenstein 2011). Several studies have also used static pictures of tools, typically opposed to pictures of animals, to assess the neural network encoding tool affordances and categorization (Martin et al. 1996; Chao et al. 1999; Chao and Martin 2000; Beauchamp et al. 2002; Rumiati et al. 2004; Fang and He 2005; Lewis 2006;

Noppeney et al. 2006; Mahon et al. 2007, 2013; Valyear et al. 2007, 2012; Vingerhoets 2008; Vingerhoets et al. 2009; Almeida et al. 2013; Mruczek et al. 2013; Garcea and Mahon 2014; Kersey et al. 2016). Only recently was an attempt made to trace the brain circuits active during tool-action observation. In functional magnetic resonance imaging (fMRI) studies, Peeters et al. (2009, 2013) showed that the observation of actual tool actions determined the activation of the classical parieto-frontal manipulation circuit (see Rizzolatti et al. 2014) and, in line with literature referenced above, a selective activation of the left anterior supramarginal gyrus (aSMG). These data indicate that tool-action observation, execution and planning share a largely common neural network, centered on the left inferior parietal lobe.

Unlike the literature for tool-action execution, data concerning tool-action observation are based mainly on fMRI studies, a technique that localizes brain activity relatively precisely, but also has a number of significant limitations (Logothetis 2008). Indeed, the neuronal activity is only indirectly measured from a hemodynamic signal, which can lead to mislocalizations, as blood oxygen level-dependent signals are biased towards the larger veins (Disbrow et al. 2000a). Recently, it was also argued that activation patterns obtained in fMRI, the result of statistical decisions on heavily averaged data, are prone to false positive when cluster level statistics are used (Eklund et al. 2016). Finally, the poor temporal resolution characterizing fMRI results impedes the ability to determine which specific event, within a complex action, activates a given brain region.

Stereo-EEG (SEEG), a technique based on intracerebral recordings (Bastin et al. 2012; Lachaux et al. 2012; Parvizi et al. 2012; Bouchard et al. 2013; Caruana et al. 2014a; Méndez-Bértolo et al. 2016), can virtually overcome all the above-mentioned issues. In SEEG, the electric activity of the cortex is recorded from several intracerebral leads implanted in individual subjects without averaging across leads, or any other smoothing. It yields local field potentials, the gamma range (50–150 Hz) of which reflects neuronal spiking activity (Manning et al. 2009; Ray and Maunsell 2011) at millisecond temporal resolution.

A limitation intrinsic to this technique is the lack of control the experimenter has over the localization of the recordings sites, as solely clinical considerations determine the implantation of electrodes. Hence, a systematic exploration of the human cortex seems impossible with this technique ("sparse sampling problem," Kadipasaoglu et al. 2014). Recently, however, it has been shown that the sparse sampling problem could be overcome by using data from many patients, pooling them by warping all the leads to a common template (Avanzini et al. 2016). Combining data from sufficiently large number of patients yields a satisfactory coverage of the human cortex.

Hence, the aim of the present study was 2-fold: (1) to trace the neural network underlying tool-action observation and (2) to characterize the selectivity of the different nodes of the tool-action observation network to the 3 selected events (video onset, action onset, and contact).

Materials and Methods

Subjects

The experiments were carried out on 49 patients (24 male and 25 female; age 30 ± 10 years old) suffering from drug-resistant focal epilepsy. The patients were stereotactically implanted with intracerebral electrodes, at the "Claudio Munari" Center for Epilepsy Surgery, Ospedale Niguarda-Ca' Granda, Milan, Italy, as part of their presurgical evaluation. Recordings were obtained from 56 hemispheres (L = 30, R = 26; bilateral = 7). The ethical Committee of Ospedale Ca'Granda-Niguarda (ID 939–2.12.2013) approved the study. Patients were fully informed of the SEEG implantation and recording procedures, and signed informed consent to participate in the study according to the Declaration of Helsinki (BMJ 1991; 302:1194). Only adults who had signed the informed consent were considered. In addition, the selection of patients have been submitted to a series of stringent precautionary measures (see Inclusion Criteria) with the specific aim of avoiding recording data from any pathophysiologically compromised brain tissue.

Subjects were recruited from a cohort of 104 patients undergoing SEEG investigation in a period from June 2012 to July 2015. Only 49 patients were enlisted for the present study, because 37 patients did not met the above-mentioned criteria, 17 were underage, and 1 patient who met the criteria refused to sign the informed consent.

Inclusion Criteria

Inclusion criteria included anatomical, neurophysiological, neurological, and neuropsychological tests. "Anatomical criteria": only patients whose MRI did not present any ischemic injury, malformations of cortical development (e.g., heterotopy, polymicrogyria, focal cortical dysplasia) or tumors were accepted for the study. The MRI of the patient was examined by experienced neurologists, neurosurgeons and neuroradiologists. "Neurophysiological criteria": this examination included the inspection of the patients EEG recorded both from the scalp and intracranially, during sleep and wakefulness. Pathological activity was characterized by the presence of epileptic discharge during the seizure, but also by the presence of epileptic spikes during interictal activity. Leads showing subcontinuous interictal pathological activity were discarded. Epileptic spikes detection was performed by expert neurologists with a long experience in intracranial EEG recording. Beside the inspection of the EEG activity at rest, the neurophysiological investigation of the sensorimotor system also included an assessment of the normal reactivity of both intracranial and scalp EEG to a large set of peripheral stimulations (somatosensory, visual, vestibular, and auditory stimulations). These were crucial to assessing the expected reactivity and normal conduction times. "Neurological and neuropsychological criteria": patients were admitted for participation to the experiment only when the clinical neurological examination and neuropsychological tests gave negative results. Neuropsychological tests evaluated the patient's competences in language (production, comprehension, reading), verbal memory, visuo-spatial memory, visual exploration, executive and attentional functions, visual perception, and abstract reasoning. "Additional criteria": recordings were performed only in the absence of seizures in the 24 h prior the experiment, with no alteration of sleep/wake cycle or additional pharmacological treatment.

Electrode Implantation and Anatomical Reconstruction

Implantation sites were selected on clinical grounds, according to ictal semiology, scalp-EEG and neuroimaging studies, and with no reference to the present experimental protocol. All the stereotactic trajectories were planned based on multimodal imaging, and the electrodes were implanted with the Neuromate robotic assistant (Renishawmayfield, Nyon, Switzerland; see Cardinale et al. 2013). They had a diameter of 0.8 mm and consisted of 8 to 18 2-mm-long contacts (leads), spaced 1.5 mm apart (DIXI). Generally, they were inserted horizontally from lateral to

medial parts of the hemispheres, but a few (1 or 2 per hemisphere) were implanted obliquely. The tip of the devices consisted of a recording lead, thus facilitating recordings and stimulations in the cortex of the mesial aspect of the hemispheres. Immediately after the implantation, cone-beam computed tomography was obtained with the O-arm scanner (Medtronic), and registered to preimplantation MRI (voxel size 0.5 × 0.5 × 2 mm). Subsequently, multimodal scenes were built with the 3D Slicer software package (Gering et al. 1999), and the exact position of leads within the 3D volume of each individual patient was determined using multiplanar reconstructions and Freesurfer (Dale et al. 1999) computed surfaces. The average number of electrodes implanted in each hemisphere was 12 ± 4, ranging from 2 electrodes (in the less explored hemisphere in the case of bilateral implantations) to 19 electrodes.

The anatomical reconstruction procedure projected all the recording leads located in the gray matter of all patients onto the fs_LR brain template (Fig. 1), following the procedure described in Avanzini et al. (2016). The procedure involved 3 steps: (1) the segmentation of MR images of each patient and the resampling of individual mid-thickness surface to match the Fs-LR-average template; (2) the identification and reconstruction of the recording leads in the 3D volume, on the basis of the CT signal, the determination of their intersection with the ribbon surface and the identification of the leads located in the gray matter of the patient; and (3) the projection of the recording leads located in the cortex of individual patients onto the Fs-LR-average template.

Paradigm

Recordings were made in a dimly lit, quiet room. The patients were sitting approximately 65 cm from the computer display on which the stimuli were presented. Stimuli were taken from previous fMRI experiments (Peeters et al. 2013). These consisted of 2.5 s videos (size 13.5 × 11.5 cm = 12° × 10°) depicting tool or hand actions, along with static frames taken from the same videos (Fig. 2). Tool actions included using a screwdriver used as an awl to pick up objects, a rake to drag objects towards the actor and pliers to lift objects. These videos were combined into a single compound tool video (TV) condition, to enhance stimulus diversity. The corresponding hand actions were grasping and dragging combined into a single hand video (HV) condition.

The experiment followed a basic 2 × 2 design, with EFFECTOR (tool or hand) and PRESENTATION MODE (video or images) as factors, generating the 4 conditions: TVs, HVs, tool images (TIs), and hand images (HI). In each condition, 12 different samples (3 tools x 2 objects x 2 actors) were randomly presented 5 times. Thus, 60 trials were presented per condition in a fully randomized order. Between trials, a uniform gray background was presented for 1 s. Patients were instructed to fixate a target in the center of the screen, without any specific task to accomplish. The fixation behavior was monitored by the neurologist supervising the experiment.

In the dynamic stimuli (TV and HV), 3 different events were used to align the gamma-power time courses across trials: (1) VIDEO ONSET: the first frame of the video in which only the object to be manipulated, but not the effector (i.e., no hand or tool), was present; (2) ACTION ONSET: the first frame in which the effector (i.e., hand or tool) appeared in the video. The latency of the action onset ranged, in different videos, from 0.00 to 0.98 s and 0.00 to 0.70 s in HV and TV, respectively; and (3) CONTACT: the first frame depicting the contact between the effector (i.e., hand or tool) and the object. The latency of the contact ranged, in different videos, from 0.70 to 1.50 s and 0.55 to 1.60 s in HV and TV, respectively.

Data Analysis

During the experiment SEEG was continuously sampled at 1000 Hz by means of a 192 channel-EEG device (EEG-1200 Neurofax, Nihon

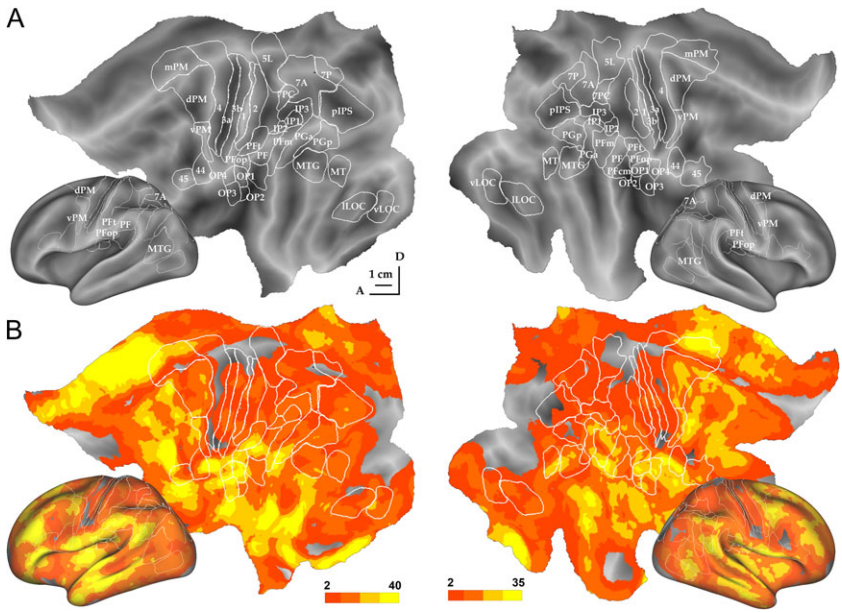

Figure 1. Anatomical maps. (A) Flat map of the fs_LR brain template with cytoarchitectonic and functionally defined areas. Cytoarchitectonic regions include somatosensory areas 6, 4, 3a, 3b, 1, 2 (Geyer et al. 2000); opercular areas (Eickhoff et al. 2007), PF areas (Caspers et al. 2006), IPS and SPL areas (Scheperjans et al. 2008), and BA 44, 45 (Amunts et al. 1999). In addition, ROIs for the posterior MTG, MTc, posterior IPS, and lateral occipital cortex were drawn to indicate the localization of leads reported in Table 2 and Supplementary Table S2. The inset shows the inflated surface of the hemispheres. (B) Sampling density of the left hemisphere computed from 3285 leads located in the gray matter. The color scale is expressed as the number of leads within a disk of 1 cm in radius and centered on each node of the mesh (Avanzini et al. 2016). Inflated surface of the hemispheres are also shown.

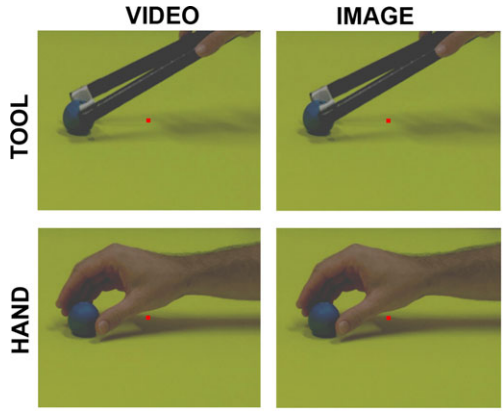

Figure 2. Experimental paradigm. Stimuli consisted of 2.5 s videos depicting tool or hand actions, along with static frames taken from the same videos. In each condition, 12 different samples were randomly presented 5 times.

Kohden). In each patient, all leads from all electrodes were referenced to a lead in the white matter far from the recording sites, in which low and high frequency electrical stimulations did not produce any subjective or objective manifestation (neutral reference). A band-pass filter (0.015–500 Hz) was applied to avoid any aliasing effect. Recordings were visually inspected by clinicians in order to ensure the absence of artifacts or any pathological interictal activity. Pathological channels were discarded. In addition, trials showing artifacts ($n < 5$ for each patient) were removed by custom-made Matlab software.

Each lead located in the gray matter was analyzed in the time-frequency domain by convolution with complex Morlet's wavelet (50–150 Hz). According to previous studies from our group (see Caruana et al. 2014a, 2014b), gamma power in the 50–150 Hz range was estimated for 10 adjacent nonoverlapping frequency bands, each 10 Hz wide. Accordingly, the term "gamma activity" throughout the text and figures describes the mean power over the entire gamma frequency range. For each condition and event, the gamma-power time course, computed over a time window from 500 ms preceding to 1000 ms following the event, was z-scored against the 500 ms interval preceding the stimulus onset. The varying relative latencies between the different events of interest allowed us (1) to compute the gamma power of each lead aligned to the 3 different events, and (2) to evaluate which event triggered the strongest gamma response.

Statistical Analysis

Responsiveness

A preliminary analysis was performed to identify responsive leads among the 5502 leads (L = 3285; R = 2217) localized in the cortical gray matter. For each lead, we evaluated the significance of gamma power (50–150 Hz) increase in four 250 ms time-bins following the event, by applying a *t*-test to postevent bins versus preevent baseline, applying a correction for multiple comparisons within a test ($\alpha = 0.0125$). The analysis was applied independently to 8 different 1500 ms intervals: those aligned to stimulus onset in the 2 static conditions (HI and TI), and those aligned to the 3 different events (video onset, action onset and contact) in the dynamic conditions (HV and TV). All leads showing a significant gamma increase in at least one condition were submitted to further analyses.

Video Deconstruction

For each lead responsive to video presentation, we determined which of the 3 events (video onset, action onset, and contact) triggered the strongest gamma response. To this end, we carried out a 2-way repeated measures ANOVA, with EVENT (3 levels: video onset, action onset, and contact) and TIME (30 adjacent 50 ms time-bins) as within-subject factors. The selection of the 3 events was based on previous evidence that these events play different functional roles, and trigger different neural activities in distinct brain regions. The distinction between video onset and action onset aimed at highlighting regional selectivity to the dynamic component of our stimuli, which could be masked by the concomitant transient due to stimulus onset. Notably, the different reactions of adjacent regions in the MT complex to motion versus flicker has been described in single neuron studies in the monkey (Lagae et al. 1994). Similarly, the specificity to action onset versus contact observation has been described in single neuron studies in the monkey motor system (Umiltà et al. 2008; Rochat et al. 2010). In addition, the role of the contact during reaching and grasping movements in representing subgoals of the task, marking transitions between action phases, has been also highlighted by a number of TMS (Cattaneo et al. 2009, 2013) and behavioral studies (see Johansson and Flanagan 2009).

The analysis was conducted independently on both tool and hand action observation. Type 1 error was controlled by applying FDR correction to the *P*-values of each interaction ($P < 0.0135$). For each lead showing a significant interaction and at least one significant main effect, post hoc analysis was conducted by means of a paired *t*-test according to a planned comparison design. Subsequent analyses were restricted to leads that showed a significant and selective responsiveness for action onset in the TVs.

Single Effect of Effector for Dynamic Conditions

To evaluate the selectivity to HV and TV observation, a 2-way repeated measures ANOVA with CONDITION (HV, TV) as between-subjects and TIME (30 adjacent 50 ms time-bins in a [–500 1000] ms window) as within-subjects factors was performed. Results were corrected for false positives by applying FDR correction to the *P*-values of each interaction ($P < 0.023$). For each lead showing a significant interaction and at least one significant main effect, post hoc analysis was conducted by means of a paired *t*-test according to a planned comparison design. In particular, this ANOVA served to indicate for each lead the possible presence of a main effect of TIME. To obtain the significant bins in the TI and HI conditions, a similar ANOVA was performed for the static conditions. All leads presenting at least a significant TIME effect for dynamic conditions, were submitted to further analysis to quantify their sensitivity to the observed effector, to the presentation mode or to their interaction.

Analysis of the Full Factorial Design

To evaluate tool actions selectivity while taking into account the dynamic/static feature of the stimuli, we applied a 2 × 2 ANOVA using factors EFFECTOR (tool, hand) and PRESENTATION MODE (static, dynamic) to all leads showing a significant main effect of time for dynamic stimuli aligned to ACTION ONSET. FDR correction for false positives was applied to the p-values of the main effect of EFFECTOR ($P < 0.0175$) and interaction ($P < 0.0075$). As the neural response to static images is much shorter relative to that following video presentation, average gamma power across significant time-bins was used as response for each of the 4

conditions, in order to maintain the ratio between static and dynamic stimuli.

Additional Factors in the Statistical Analysis

The statistical analyses described above assume that the leads of the electrodes in the different patients are independent. One can thus question to what degree the lack of consideration of effects of such factors as hemisphere, patient, or electrode inflated the results' significance. The number of patients with recordings from both hemispheres was small (7 out of 49 patients) and in 3 of these the placements were extremely unsymmetrical with only 2 electrodes (about 20 leads) recording from the secondary hemisphere. Thus, the 2 hemispheres were analyzed separately as almost 90% of the hemispheres were independent.

The factor "patient" is potentially more relevant. The implantation of electrodes in different patients, dictated by the clinical needs, varies widely, with some implantation patterns showing no overlap at all. This is illustrated in Figure 3 showing the leads located in the gray matter of the most (yellow) and least (black) responsive subjects in the deconstruction of video analysis (see Supplementary Table S1). This lack of overlap prevents any spatial smoothing from creating enough overlap to consider the factor patient in the analysis. Furthermore, the responsiveness of leads largely reflected their anatomical localization. The proportion of responsive leads in the video deconstruction analysis correlated strongly with the percentage of leads located in a posterior mask (reddish hatching in Fig. 3) including parietal, occipital cortex, posterior frontal cortex and ventro-posterior temporal cortex, explaining 56% of the variance in responsiveness. Thus considering the factor patient in the analysis may spuriously remove most of the effects of lead localization, which are the very target of the present study. Despite this expected and informative variability, it is worth noting that all patients contributed a substantial percentage of leads to the population analysis (ranging from 28% to 84% in Supplementary Table S1), excluding that the results reflect a bias due to a few subjects.

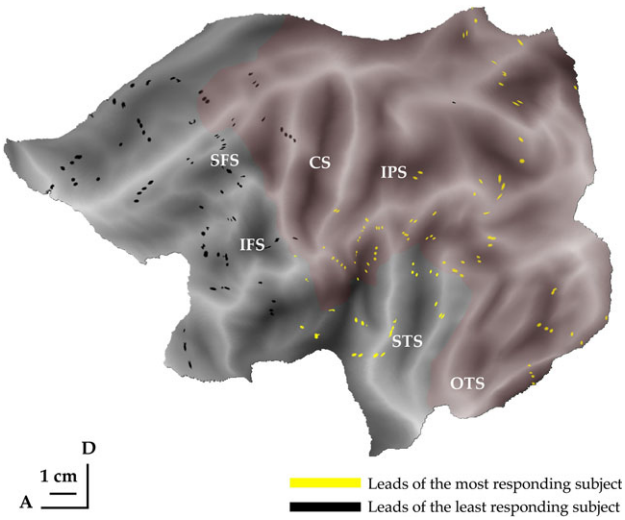

Figure 3. Flat map of the left hemisphere showing the leads located in the gray matter of the most (yellow) and least (black) responsive subjects in the video deconstruction analysis, showing the correlation between patient overall responsiveness and anatomical localization of its implantation. The reddish hatching indicates the posterior mask used to calculate the proportion of responsive leads located in the posterior areas, as indicated in Supplementary Table S1.

Finally, the factor "electrode" may seem the most important as passive volume conduction is likely to create spurious correlations between adjacent leads on an electrode. Therefore, we evaluated both the frequency of occurrence of adjacent leads exploring cortex and the correlation between such leads. We estimated the proportion of adjacent leads to be 36% of the selective leads in the video deconstruction analysis and 25% in the full factorial analysis. These percentages, however, overestimates the number of nonindependent leads as indicated by the computation of the correlation matrices, shown for 2 patients in Figure 4. Correlations between leads were calculated over the entire duration of the tool/hand action test (≈17 min) with a bin width of 50 ms. Inspection of these matrices yields 2 important observations. First, any correlation between "next-to-adjacent" leads (i.e., leads separated by one or more intervening leads) of the same electrode are very small and generally explain less than 10% variance. Hence, to calculate the number of independent leads for a sequence of n successive leads located in cortex, one should solely remove the extreme leads, which may be subject to passive volume conduction. This yields $n - 2$ independent leads, a much larger value than that obtained by simply subtracting the number of adjacent pairs ($n = 1$) from n, which trivially yields one. For short sequences (equal or shorter than 3) this makes no difference but for an electrode with 8 successive leads in the cortex, and thus 7 adjacent pairs, as electrode M in Figure 4A, it does: the number of independent leads is not 1 ($8-7 = 1$), but $8-2 = 6$ leads. Although most sequences of successive leads were short, this observation qualifies the percentage of adjacent leads amongst the selective ones, as it implies that the proportion of independent leads exceeds 70% in the video deconstruction and 75% in the full factorial analyses. The second observation is that the degree of correlation between "adjacent" leads can vary considerably between electrodes and patients, with a quarter rather small (less than 15% explained variance). Passive volume conduction cannot account for such a variability as it predicts that all adjacent leads should show similarly strong correlations. Instead, the variability in the correlations strongly supports the view that they largely reflect local connections and/ or functional similarities between adjacent leads located in the same anatomical or functional region. These analyses indicate that the inclusion of the factor electrode in the statistical analysis of the present study is not warranted.

Localization

All leads showing significant effects in one of the previous analyses were related to a priori regions of interest (ROIs), defined in previous studies (Fig. 1A). Cytoarchitectonic regions include somatosensory areas 6, 4, 3a, 3b, 1, 2 (Geyer et al. 2000); opercular areas (Eickhoff et al. 2007), PF areas (Caspers et al. 2006), IPS and SPL areas (Scheperjans et al. 2008), and BA 44, 45 (Amunts et al. 1999). The MT cluster (MTc) ROI was adapted from the retinotopically defined MT cluster by Abdollahi et al. (2014). In addition, ROIs for the posterior MTG, posterior IPS, and lateral occipital cortex were drawn on the flat maps to indicate the localization of leads reported in Table 2 and Supplementary Table S2.

Results

Database

Recordings were obtained from 5502 recording leads ($L = 3285$; $R = 2217$; see Table 1) located in the cortical gray matter. The sampling density maps computed for the 2 hemispheres (Fig. 1B; see Avanzini et al. 2016) shows the recording coverage of cortical sheet, with high densities located bilaterally in the

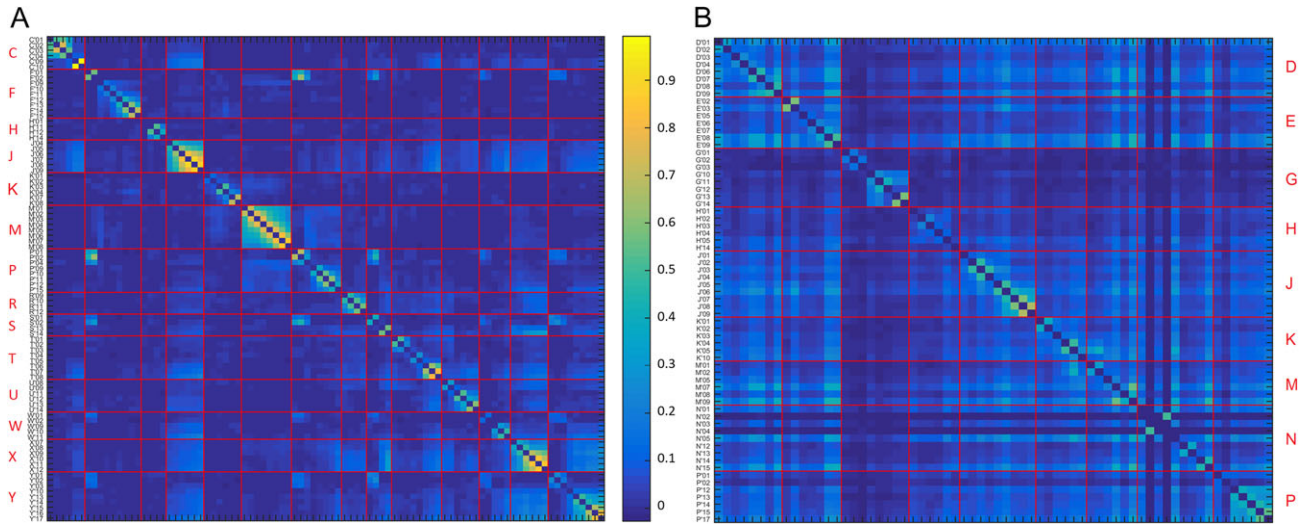

Figure 4. Correlation matrices in 2 patients. Panels show the correlation matrices computed for 2 different patients overall leads exploring gray matter. Pearson correlation coefficient (r) was computed on the continuous gamma power (about 17 min of recording, power time course sampled each 50 ms) averaged in the frequency band between 50 and 150 Hz, and masked for its significance ($P < 0.05$, uncorrected). Red lines indicate the separation between the different electrodes, whose main letter (see Materials and Methods) is indicated aside in red.

anterior cingulate cortex, the fronto-parietal operculum, the middle temporal gyrus, the mesial temporal region and the middle and superior frontal gyrus. The frontal and occipital tips of the hemispheres and the cortical crowns were poorly represented because of the obligatory orthogonal insertion of electrodes and the anatomical and vascular constraints. A total of 2618 (L = 1547; R = 1071) leads located in the gray matter showed significantly increased gamma activity in at least one of the conditions (see methods) relative to the baseline, as assessed by preliminary t-test (see Materials and Methods), and were subjected to further analyses.

Video Deconstruction for Tool-Action Observation

Once the leads active during the task were established, we determined, for each of them, which of the 3 event alignments (tool VIDEO ONSET, tool ACTION ONSET, and tool CONTACT) triggered the strongest gamma response during tool-action observation (Fig. 5A). The analysis was carried out for the 2618 leads (L = 1547; R = 1071), which passed the preliminary test (see above). A representative example of each category is shown in Figure 5B. Supplementary Table S1 indicates that all patients contributed to these results.

The tool VIDEO ONSET was the optimal alignment for 171 leads (L = 96; R = 75). These leads were equally distributed across the 2 hemispheres (χ^2 $P > 0.05$), and clustered in the lateral occipital cortex, posterior collateral sulcus and lingual gyrus, posterior IPS, IP3 and left precuneus (Fig. 6, upper panel; see also Supplementary Figs S1 and S2 and Table 2).

The tool ACTION ONSET was the best alignment for a large number of the responsive leads (n = 331. L = 236; R = 95). The distribution of these leads was strongly left lateralized (χ^2 $P < 0.001$). It included the ventral part of the lateral occipital cortex, MTc, posterior MTG, posterior IPS, and PFt in the IPL. In the frontal lobe, these leads were clustered in ventral and dorsal PMC and, to lesser extent, in frontal area 46 (Fig. 6, middle panel; see also Supplementary Figs S1 and S2 and Table 2).

A few leads (n = 23. L = 9; R = 14) showed a statistically significant increases in gamma power when aligned to the tool CONTACT. These leads were mainly clustered in the dorsal PMC and the parietal operculum OP1, corresponding to area SII, and were equally distributed between the 2 hemispheres (χ^2 $P > 0.05$; Fig. 6, lower panel; see also Supplementary Figs S1 and S2 and Table 2).

Finally, the majority of the leads (n = 2093. L = 1206; R = 887) failed to show any significant selectivity for a specific alignment. These unselective leads were equally balanced in the 2 hemispheres (χ^2 $P > 0.05$).

Table 1. The number of patients, and recording and responsive leads, as well as the average P-values and SD of the interaction (inter.), in the 3 ANOVAs reported in the Results. Main effects (m.e.) of interest are also reported

	Left	P values	Right	P values
Patients	30		26	
Recording leads	3285		2217	
Responsive leads	1547		1071	
Video deconstruction				
Video onset	96	0.001 ± 0.002	75	0.000 ± 0.001
Action onset	236	0.001 ± 0.002	95	0.000 ± 0.001
Contact	9	0.004 ± 0.005	14	0.001 ± 0.002
None	1206	0.429 ± 0.335	887	0.440 ± 0.336
Selectivity TV versus HV				
TV > HV	90	0.003 ± 0.005	22	0.003 ± 0.006
HV > TV	10	0.003 ± 0.005	8	0.000 ± 0.001
Time (m.e.)	133	0.270 ± 0.288	60	0.298 ± 0.300
None	3	0.118 ± 0.072	5	0.258 ± 0.255
Factorial analysis				
(m.e.) Tool	84	0.003 ± 0.005	13	0.003 ± 0.004
(m.e.) Hand	13	0.005 ± 0.005	12	0.001 ± 0.002
(inter.) Tool action	36	0.001 ± 0.001	14	0.001 ± 0.001
(inter.) Hand action	7	0.003 ± 0.003	4	0.000 ± 0.000

Tool Action Selective Regions

Selectivity to Tool versus Hand Actions

About one-third of the 331 leads presenting the strongest response when aligned to the tool ACTION ONSET showed a

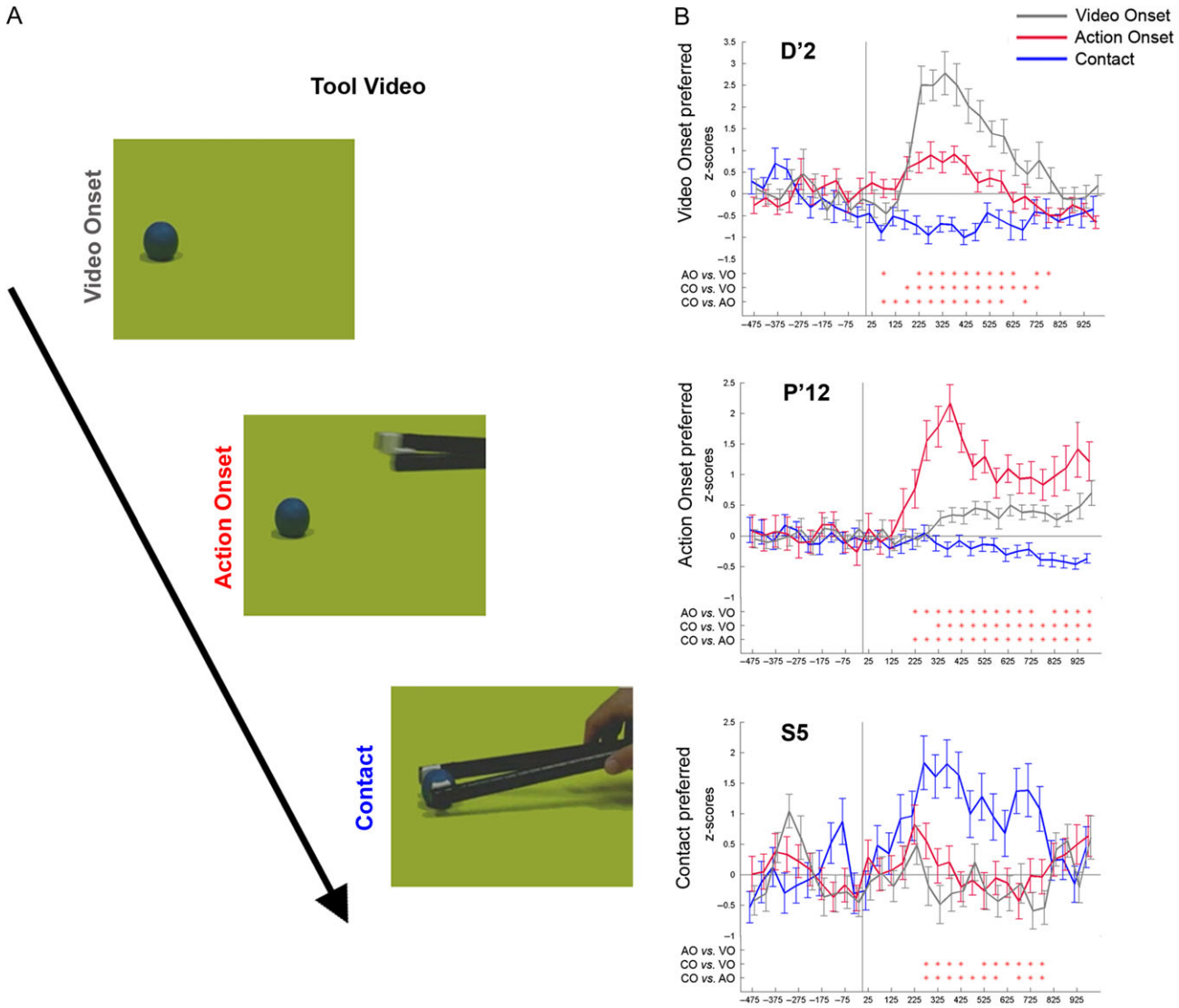

Figure 5. Events deconstruction. (*A*) Definition of the 3 events: Video Onset, Action Onset, and Contact. (*B*) Representative leads preferring alignment to video onset (lead D'2, top, located in the left lateral occipital cortex), action onset (lead P'12, middle, located in left PFt) and contact (lead S5, bottom, located in the right OP1). For each lead the gamma power (50–150 Hz) is plotted in 50 ms time-bins over the [–500 1000] ms window, during video onset (black), action onset (red) and contact (blue) alignments. In all 3 leads, *P* values for the main effect of Time (T), Condition (C), and their Interaction (C*T) were $P < 0.001$. Significant time-bins are indicated for each pairwise comparison by red asterisks in the lower part of the figure. AO, action onset; VO: video onset; CO: contact.

significant TV > HV main effect ($L = 90$; $R = 22$). These leads were mainly distributed in left PFt, left posterior IPS, left ventral PMC/44 and bilateral dorsal PMC (Fig. 7A, red dots, and Supplementary Table S2). Only a few leads ($L = 10$; $R = 8$), mainly located bilaterally in MTG and MTc, showed a significant HV > TV main effect (Fig. 7A, blue dots, and Supplementary Table S2). Finally, the large majority of leads ($L = 133$; $R = 60$) showed no significant differences between tool and hand action, indicated by a main effect of time ($P < 0.05$) without main effect of condition, nor interaction. These unselective leads were mainly located bilaterally in MTG and MTc, in the ventral part of the lateral occipital cortex, along the IPS, in dorsal and ventral PMC and frontal area 46 (Fig. 7A, black dots, and Supplementary Table S2; see also Fig. 5B for representative leads from each category). The remaining leads ($L = 3$; $R = 5$) did not show any significant main effect (see Supplementary Table S2).

Factorial Design

To further characterize the selectivity of the recording leads for observing tool actions and to investigate whether that selectivity was specific only for tool action or, for actions and static images more generally, we applied a factorial design using EFFECTOR (tool, hand) and PRESENTATION MODE (static, dynamic) as factors. We overcame the time-course difference of responses to dynamic versus static visual stimuli in SEEG by restricting the analysis to the time-bins showing a significant gamma modulation in the single effects (see Methods). This analysis was again applied to all leads which aligned best to ACTION ONSET in the TVs ($n = 331$).

A main effect of EFFECTOR, with tool > hand, was found in 97 leads ($L = 84$; $R = 13$) lying in different sectors of left IPL including PFt, the rostral part of the anterior IPS (IP2) extending into dorsal part of PF, and posterior IPS. Outside the left IPL/IPS,

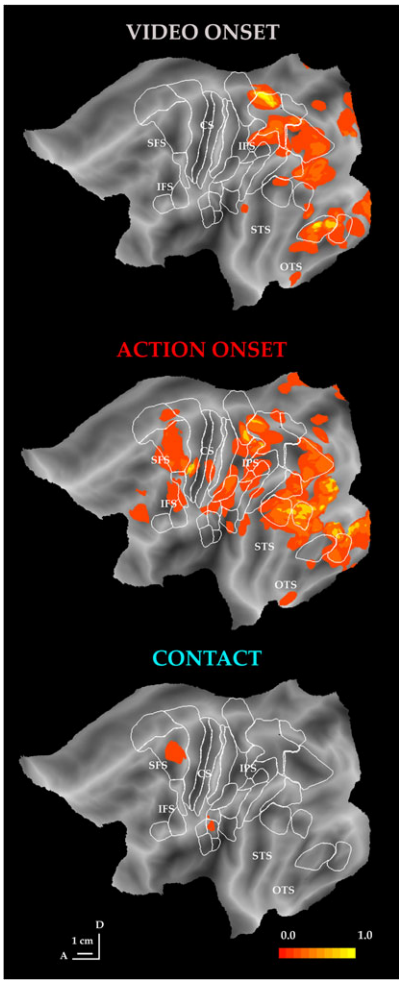

Figure 6. Responsiveness maps. Proportion of leads significantly selective to the Video Onset, Action Onset, and Contact, out of the overall number of recording leads, is plotted on the left flat surface of the fs_LR brain template. A color scale indicates the percentage of responsive leads within a disk 1 cm in radius and centered on each node of the mesh. Abbreviations: SFS, superior frontal sulcus; IFS, inferior frontal sulcus; CS, central sulcus; IPS, intraparietal sulcus; STS, superior temporal sulcus; OTS, occipito-temporal sulcus.

leads showing a main effect of tool were also found in the left posterior MTG, MTc, ventral part of the left lateral occipital cortex and bilateral dorsal PMC (Fig. 8A and Supplementary Fig. S3A, red dots). A main effect of EFFECTOR with hand > tool was found in 25 leads ($L = 13$; $R = 12$) lying in a subsector of posterior MTG bilaterally, posterior to the region where a main effect of tool was found, and MTc. Few leads were located in the posterior intraparietal sulcus (Fig. 8A and Supplementary Fig. S3A, blue dots; see also Supplementary Table S2). The remaining 209 leads did not show a main effect of EFFECTOR.

The INTERACTION between the 2 factors showed that tool-action observation triggers a stronger gamma increase than the other conditions in 50 leads ($L = 36$; $R = 14$) mainly in the left hemisphere. These leads were located mainly in the left PFt, left ventral PMC and bilateral dorsal PMC (Fig. 8B and Supplementary Fig. S3B, green dots). Notably, these data suggest that while the rostral sector of the anterior IPS is active during the observation of both tool actions and tool pictures, the PFt, lying ventral and rostral to it, is more involved in the observation of tool actions, thus suggesting a dorsal to ventral shift from the encoding of tool identity to that of tool actions. Supplementary Fig. S4 illustrates this dorsal to ventral shift in a single patient, showing leads responsive to both tool and tool action in the dorsal PFt, and leads selective only to tool action ventrally. Interestingly, the pattern of correlations (Supplementary Fig. S4C) supports the bipartite segregation with lead X'9 being the link between the 2 parts. However, the correlations between adjacent leads were smaller in the dorsal than the ventral part, even if responses were rather similar in these 2 parts. Further investigation with correlations restricted to single conditions of the design may be able to clarify the relationship between correlations and functional similarities. Only 11 leads ($L = 7$; $R = 4$) showed a reverse interaction, that is, a selectivity for hand action (Fig. 8B and Supplementary Fig. S3B, black dots). These leads showed a scattered and weak distribution, mainly around the right posterior MTG.

Regions Selective for Observing Contact

An additional analysis was carried out to investigate whether leads encoding CONTACT events during "hand" actions observation were localized in the same areas as those encoding CONTACT events during the observation of *tool* actions. We used the same procedure employed for the observation of tool actions (see "Video Deconstruction for Tool-Action Observation"). The analysis was carried out on 2618 leads ($L = 1547$; $R = 1071$), which passed our preliminary test. As in the case of tool-action observation, a few leads ($n = 35$. $L = 12$; $R = 23$) showed a statistically significant increase in gamma power when aligned to the CONTACT. These leads were clustered in the same regions where they have been found when analyzing tool actions, namely the dorsal PMC and the parietal operculum OP1. They were slightly right-lateralized (χ^2 $P = 0.003$. Fig. 9, right panel).

Discussion

In the present study, we deconstructed the observed actions into 3 events—video onset, action onset, and contact—and assessed their relative neural responses. By aligning the responses to video onset, we found activations in a large number of visual areas. By aligning the responses to the onset of the tool action, we found the activation of the classical parieto-frontal manipulation circuit (see Rizzolatti et al. 2014) and, most interestingly, a selective activation of the left cytoarchitectonic PFt (Caspers et al. 2006), largely corresponding to the tool-action observation region described by Peeters et al (2009, 2013) in aSMG. Finally, our findings indicate that the observation of the main goal of the observed action, represented by the contact between the tool and the object, elicits responses in SII and dorsal PMC. These findings are discussed in turn below.

Responses to Distinct Events

By aligning the gamma-power modulation to the 3 basic temporal events, we were able to show that each of these triggers neural activity in a different set of cortical areas.

The "video onset" is the least specific event, corresponding to the switch from the gray background to the first frame of the video, depicting a graspable object on a green background. Thus, it includes both lower order features such as luminance, contrast, orientation and color changes, and the object to be grasped. Indeed leads responding to this event were located in early visual areas (V1–3) bilaterally, and specifically in their peripheral field representations, these being the only parts explored for clinical purposes. In addition, the presence of a

Table 2. How many patients and leads contributed to the responsiveness of each ROI depicted in Figure 2. In addition, the number of leads presenting a selectivity for Video Onset, Video Action, and Contact is also reported

ROI	Left					Right				
	No. of patients	No. of leads	Onset	Action	Contact	No. of patients	No. of leads	Onset	Action	Contact
BA1	7	13	0	1	0	7	10	0	1	0
BA2	8	33	0	0	0	10	23	0	0	2
BA3a	9	20	0	0	0	6	13	0	2	0
BA3b	8	26	0	2	0	7	19	0	2	0
BA4	8	26	0	2	2	9	22	0	0	0
BA44	13	39	0	1	0	11	26	0	0	0
BA45	11	28	0	0	0	10	23	0	2	0
BA5Ci	2	2	0	0	0	0	0	0	0	0
BA5L	5	11	2	3	0	2	4	0	0	0
BA7A	5	32	13	8	0	5	9	1	4	0
BA7P	3	7	0	0	0	2	4	0	0	0
BA7PC	3	6	0	2	0	3	5	0	2	0
IP1	4	8	0	1	0	4	7	0	0	0
IP2	4	10	0	2	0	3	4	0	1	0
IP3	6	15	4	2	0	3	7	0	0	0
OP1	13	42	0	1	2	8	21	0	0	1
OP2	5	9	0	0	0	4	8	0	0	0
OP3	11	30	0	0	0	4	7	0	0	0
OP4	12	30	0	0	1	8	21	0	0	0
PF	17	63	0	9	0	12	26	0	0	1
PFcm	9	35	0	2	0	5	17	1	0	3
PFm	9	35	0	0	0	11	32	0	2	1
PFop	10	23	0	2	1	8	24	0	1	0
PFt	11	36	0	14	0	9	17	0	0	1
PGa	9	41	1	1	1	8	17	0	1	0
PGp	9	45	1	11	0	6	21	0	0	0
PMd	14	91	0	14	3	14	92	0	14	4
PMm	15	67	0	2	0	13	53	0	2	0
PMv	14	32	0	3	0	11	29	1	1	0
pIPS	8	62	15	23	0	5	11	3	0	0
MTc	10	27	0	23	0	8	21	3	10	0
MTG	9	32	1	16	0	7	41	1	15	0
vLOC	9	43	11	23	0	7	16	8	3	0
latLOC	8	34	17	1	0	11	36	26	4	0

graspable object explains the presence of active leads in a variety of shape-sensitive regions, that is, the IPS, as well as the fusiform gyrus and neighboring collateral sulcus, corresponding to the shape-sensitive region described as LOC (Kourtzi and Kanwisher 2001; Denys et al. 2004; Sawamura et al. 2006).

Unlike the video onset, the "action onset" triggered activity in the MT cluster (Kolster et al. 2010), a finding consistent with the well-known preference of this cluster for motion stimuli (Zeki et al. 1991; Dumoulin et al. 2000; Huk and Heeger 2002). This motion processing is presumed to be the starting point for the extraction of visual action responses (Nelissen et al. 2006; Jastorff et al. 2012). Action onset also activated the occipito-temporal, parietal and premotor regions. These regions included (1) posterior MTG and fusiform gyrus, at the occipito-temporal level; (2) regions along the IPS and IPL, at the parietal level, and (3) ventral and dorsal premotor cortex (PMC), extending onto the crown of the precentral gyrus. This network corresponds to the action observation/execution network (see Caspers et al. 2010; Grosbras et al. 2012; Molenberghs et al. 2012; Rizzolatti et al. 2014), which is known to house mirror neurons in the monkey (Rizzolatti et al. 2001, 2014). This circuit is most likely evolutionarily old, and possibly mediates the identification of the basic goal of the observed action in both humans and monkeys. Results show a left lateralization of this network. The trajectory of the hand cannot explain the results because it started from the right visual field (left hemisphere), but then moved to the left visual field (right hemisphere). In addition, the "contact" points always occurred in the left visual field, but the activation was present in both hemispheres. Finally, the return movement started in the left field and ended in the right. Thus, the explanation of the lateralization in terms of visual field cannot account for the data. In addition, as described in the methods, only actions made by the right hand, moving from the right to the left visual field, were shown to the patients. The possible effect of the left versus right hand on the lateralization was previously investigated by Johnson-Frey et al. (2005) in a study of tool-action planning, and by Moll et al. (2000) in a study of tool-action pantomime. In both studies, tool use actions activated a left-lateralized network for either limb, which largely overlaps the one described here.

The "contact" between the tool and the target object triggered activity in 2 brain regions, the dorsal PMC and the parietal opercular region OP1, corresponding to human SII (Eickhoff et al. 2007). The possibility that these 2 regions, albeit triggered by the same event, encode different information concerning the tool-object interaction, is discussed below. These responses

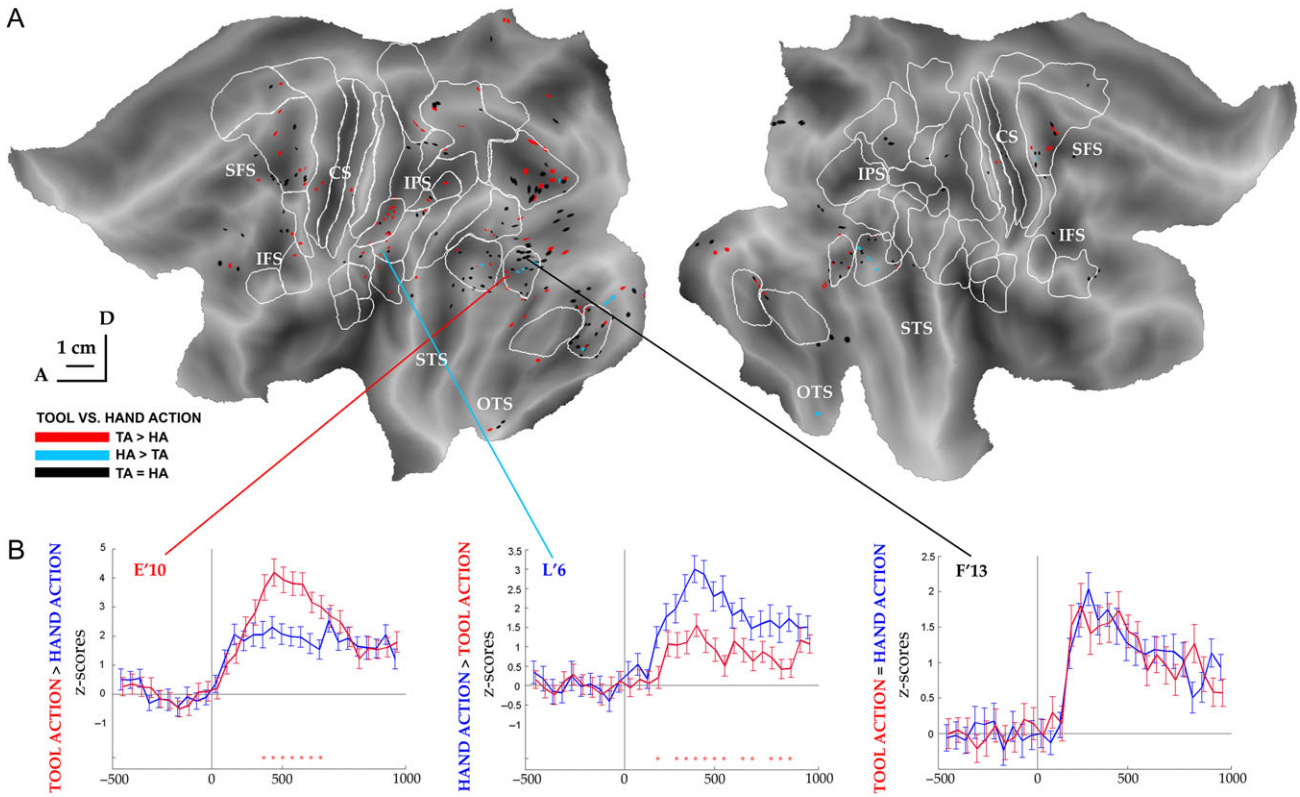

Figure 7. Selectivity for tool versus hand actions. (*A*) Dots represent recording leads showing a significantly stronger increase in gamma power during the observation of tool action (red dots) or hand action (blue dots), or an equal responsiveness to both stimuli (black dots). Abbreviations as in Figure 4. (*B*) Representative leads for the 3 categories. Lead E'10, selective for tool-action observation, was located in the left MTc; lead L'6, selective for hand action, was located in the left PF; lead F'13, showing equal responsiveness to both stimuli, was located in the left MTc. In all leads, *P* values for the main effect of Time (T), Condition (C), and their Interaction (C*T) were $P < 0.001$. Same conventions as in Figure 3B.

to contact, which escaped the previous fMRI studies (Peeters et al. 2009, 2013), demonstrate that action observation, similar to action execution, is a dynamic process during which different brain regions become sequentially active over time (see Fig. 6), hence requiring a time resolved technique to be studied and characterized.

The Specificity of the aSMG for Tool-Action Observation

The present study reveals the presence of 2 sets of leads responding to tools. One exhibiting strong responses to tool actions and static pictures of tools, whereas both were significantly stronger relative to the corresponding hand conditions. These leads were located in several locations, and specifically in pMTG, posterior IPS, IPL and PMC. These findings are in full agreement with a large body of brain imaging studies (Martin et al. 1996; Chao et al. 1999; Chao and Martin 2000; Rumiati et al. 2004; Fang and He 2005; Lewis 2006; Noppeney et al. 2006; Mahon et al. 2007, 2013; Valyear et al. 2007, 2012; Vingerhoets 2008; Vingerhoets et al. 2009; Almeida et al. 2013; Mruczek et al. 2013; Garcea and Mahon 2014; Kersey et al. 2016; Kellenbach et al. 2003; see Johnson-Frey 2004; Orban and Caruana 2014; Reynaud et al. 2016). A second set of leads responded to the observation of tool actions, but not to the observation of static tools. These action related leads were present in various areas but concentrated in cytoarchitectonic area PFt. Both sets of tool responsive leads showed a clear left hemispheric bias. Note that the fMRI studies by Peeters et al (2013) revealed only tool-action activations, because the static frames were used as a control condition, preventing an evaluation of the balance between main effect and interaction in the different cortical regions.

A comparison of the location of the leads responding exclusively to tool action with that of leads also responsive to static tools, showed a distinction between the dorsal (posterior) third of PFt, where the latter predominated, and its ventral (anterior) two-thirds in which tool action dominated. It is likely that the ventral two-thirds correspond functionally to aSMG of Peeters and coworkers, although the conjunction analysis of all tools used in those studies showed an anterior shift compared with the current data. In fact, some of the leads recording exactly from the conjunction-defined fMRI region were unresponsive, unlike those located just ventral to it (Fig. 10). It is possible that the localization of aSMG proposed in the previous fMRI studies may have been slightly biased towards the veins located in the postcentral sulcus, as has been previously observed in the monkey (Disbrow et al. 2000a). Independently of the detailed subdivision of the rostral IPL, it is interesting to note that as one moves ventrally towards the parietal operculum, responsiveness to both static and dynamic stimuli give way to the observation of dynamic stimuli only. Finally, in OP1 the alignment to the contact predominates. This spatial order mirrors the temporal order of the events in the TVs.

It is of interest to compare our data with the results by Chao and Martin (2000) and Mahon et al. (2007). The former authors studied the areas active during viewing and naming pictures of tools. They found, in addition to activation of the temporal lobe (see also Chao et al. 1999), parietal and premotor activations.

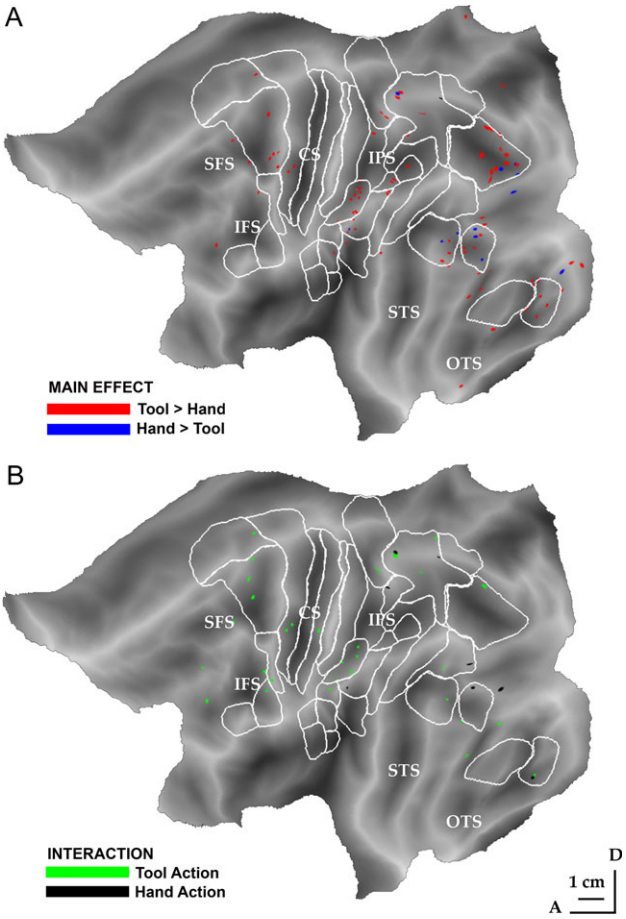

Figure 8. Analysis of the full factorial design comparing tool and hand responses. (A) Leads showing a main effect of EFFECTOR (tool, hand) in the left hemisphere. Red dots: main effect of tool; blue dots: main effect of hand. (B) Leads showing an interaction between EFFECTOR (tool, hand) and PRESENTATION MODE (video, images). Green dots: Tool action selective leads; black dots: hand action selective leads. Abbreviations as in Figure 4.

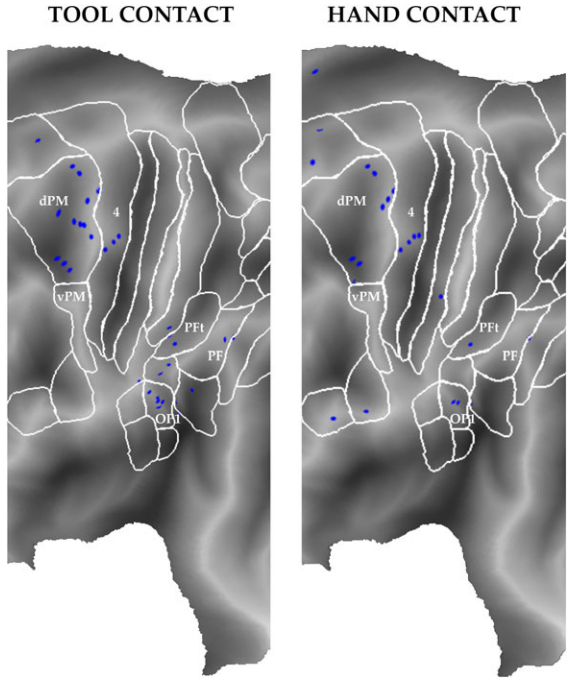

Figure 9. Leads responsive to the tool and hand contact. Leads selective for the contact between the tool and the object (left) and between the hand and the object (right). All leads are shown on the left fs_LR template.

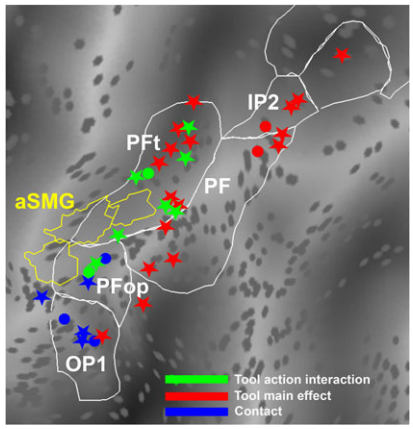

Figure 10. Recording leads in PFt and surrounding regions. White outlines indicate cytoarchitectonic areas, yellow outlines indicate aSMG defined by Peeters et al (2013). Red and green dots depict leads showing a significant alignment for the action onset and a main effect for tools (red) or an interaction for tool action (green). Blue dots indicate leads showing a significant alignment for the contact. For all categories, leads showing significant activity after FDR correction are indicated by stars, while others (uncorrected $P < 0.05$) are indicated by circles. Gray dots indicate nonresponsive leads.

This finding is in close agreement with our data, which show a main effect of tool in both inferior parietal and PMC. Of great interest also is the subsequent article by Mahon et al. 2007 regarding the role of the parietal lobe in shaping object representation in the ventral stream. Based on fMRI study, these authors proposed that tools identification in the temporal lobe is shaped by tool use processing in the left inferior parietal lobule. In addition, by comparing patients with inferior parietal and temporal lesions, Mahon and coworkers reported that there was a reliable relationship between performance in tool use and tool identification only in the group of patients with lesions involving the parietal cortex. This finding is in line with our data that the increased gamma power in dorsal PFt also occurs during observation of static tools, and not exclusively during tool-action observation. Thus, the dorsal sector of PFt should be responsible for tool identification in IPL, while the temporal sectors should play a crucial role in shaping object representation in the ventral stream.

It is obvious that in order to tune the temporal lobe organization to the proper use of the tool, a real executed action should have occurred. The findings of Brandi et al. (2014), showing that the same inferior parietal region described above became specifically active during tool use, strongly support this hypothesis. In addition, they indicate that action observation is a useful proxy for studying real action execution, given the close neural similarities between action execution and action observation.

An open question concerning the role of the area PFt in tool use is whether it contributes to the "mechanical reasoning" characterizing tool selection and use (Goldenberg and Hagmann 1998; Osiurak et al. 2010; Osiurak and Badets 2016) or if it is involved in the storage of manipulatory knowledge about how to manipulate tools, as classically maintained (Buxbaum 2001). The current study does not address this issue explicitly,

as it provides information related to localization of tool use observation, and not on the mechanism underlying tool use. We note, however, that these interpretations are substantiated mainly by neuropsychological evidence from left parietal lesions, which typically involve large areas of cortex. Our study, on the other hand, highlights a high degree of specialization in the various IPL subregions (e.g., IPS, PFt, PFop, OP1), which is compatible with the hypothesis that different tool-related processes rely on the integration of signals from distinct, albeit adjacent, IPL sectors (Caruana and Cuccio 2017).

The Activity of PMC During Tool and Hand Action Observation

A number of task-related leads responsive to both static and dynamic tool stimuli were located in PMC. As far as responses to static stimuli are concerned, they confirmed previous data by Grafton et al. (1997) and Chao and Martin (2000), who demonstrated that the observation of static tools activates both dorsal and ventral PMC. As suggested by these studies, this activation could be related to canonical neurons described in the monkey (Murata et al. 1997), and most likely present also in humans.

As for the responses to dynamic stimuli, they are in accord with a vast literature covering both monkeys and humans showing that observing goal-related actions triggers the activation of the PMC (Gallese et al. 1996; Rizzolatti et al. 1996; see Caspers et al. 2010; Grosbras et al. 2012; Molenberghs et al. 2012; Rizzolatti et al. 2014). This activation is likely related to the activity of mirror neurons recorded in monkey. Of particular interest for the present discussion are the data by Rochat et al. (2010) who showed that mirror neurons responding to the observation of hand grasping also responded to the observation of grasping with pliers, and many of them even to the observation of spearing with a stick. These data have a counterpart in human experiments (Cattaneo et al. 2009, 2013). Cattaneo and coworkers recorded the motor-evoked potentials (MEPs) to TMS from the right opponens pollicis (OP) muscle while participants observed an experimenter operating 2 types of pliers: normal and reverse pliers. By using this paradigm, the authors were able to dissociate action goals and movements. The results showed that during the observation of actions performed with both types of pliers, the MEPs from OP were modulated by the action goal, and not by the movements.

The current data also accord with some findings by Peeters et al. (2009) regarding tool-action observation. These authors found that the presentation of both hand and tool actions triggered activity in the PMC, as well as in the action observation/execution network. However, in their study, the contrast of tool versus hand action observation showed that large part of this activation was determined by grasping in general, and not specifically by tool action. An exception was found in the case of actions performed with a screwdriver used as an awl, which reached significance relative to hand action.

Contact

Johansson and Flanagan (2009) have emphasized the importance of contact events between digits and objects as sensorimotor control points for the reaching component in reach-to-grasp actions and manipulation in general. Furthermore, they argued that while tactile feedback information is essential for skilled object manipulation, the visual system might also monitor contact events. They based this conclusion on the eye shifts during observation of skilled manipulation (Johansson et al. 2001). Indeed, the fact that the gaze shifts to the goal of the next action phase around the predicted time of goal completion suggests that the visual system can predict and monitor contact events representing subgoal completion. In the present study, the vision of the object touched by the hand, or by the tool, yielded responses in 2 very specific regions: OP1, corresponding to SII (Disbrow et al. 2000b; Eickhoff et al. 2007), and dorsal PMC, suggesting a possible implementation of this visual contact monitoring. SII is classically a somatosensory area responsive mostly to tactile stimuli. Recently, it has been found that a consistent percentage of neurons in SII is selectively activated during object manipulation and grasping (Ishida et al. 2013). Most interestingly, Hihara et al. (2015) found that approximately one-third of the neurons in SII responded to visual stimuli. Typically, these neurons required complex stimuli, among which was the observation of human actions. These data are in agreement with previous brain imaging data in humans, which have documented an activation of SII by the vision of persons being touched (Keysers et al. 2004; Blakemore et al. 2005; but see Chan and Baker 2015) and by observing skin being moved (Ferri et al. 2015).

While these findings might explain our results as far as the hand contact is concerned, one may wonder why the same activation pattern returns during the observation of the tool-object contact. An explanation may be found in the experiment by Iriki et al. (1996). These authors demonstrated that the actions performed by the monkey with a tool determined the embodiment of the used tool in the body schema of the agent (Iriki et al 1996). Indirect evidence suggests a similar effect in humans (see Maravita and Iriki 2004 for a review). It is possible therefore, that a similar embodiment might explain why, in our study, the observation of the tool contact with an object produced the same effect as during the observation of hand-object contact.

Finally, contact alignment also activated dorsal PMC and in the primary motor cortex. Although mirror neurons are typically recorded in the monkey ventral PMC and the ventral part of dorsal PMC (F2vr), fMRI meta-analysis in humans (Caspers et al. 2010; Grosbras et al. 2012; Molenberghs et al. 2012) showed that during action observation there is also a strong activation of the dorsal PMC. Because fMRI cannot distinguish among the events composing reach-to-grasp actions (i.e., reaching, hand shaping, actual grasping and contact with the object), it is difficult to establish what types of neurons are responsible for dorsal PMC activation. The present finding indicates that both the dynamic aspects (reaching and grasping) and the contact are present in dorsal PMC. A recent TMS study (Davare et al. 2006) suggests that dorsal PM controls the coupling the grasping and reaching phases of reach-to-grasp actions. The present study suggests that dorsal PM may also represent this contact event visually, as may primary motor cortex, in which mirror neurons have also been reported (Vigneswaran et al. 2013; see also Kraskov et al. 2014).

Conclusions

Exploiting the temporal resolution of the SEEG allowed us to highlight the selectivity of different human brain regions to different events composing tool and hand action observation, starting from the appearance of the object, followed by action onset, and ending with the attainment of their goal. Both tool and hand actions activated the basic action observation

network, but only tool actions activated the left aSMG, largely corresponding to cytoarchitectonical area PFt.

Supplementary Material

Supplementary material is available at *Cerebral Cortex* online.

Funding

We thank Ivana Sartori for the invaluable technical support. This study was supported by European Research Council (ERC) "Cogsystem" project no. 250013 (to G.R.) and "Parietalaction" project no. 323606 (to G.A.O.) and by a grant from Fondazione Cariparma (to G.R).

Notes

Conflict of Interest: None declared.

References

Abdollahi RO, Kolster H, Glasser MF, Robinson EC, Coalson TS, Dierker D, Jenkinson M, Van Essen DC, Orban GA. 2014. Correspondences between retinotopic areas and myelin maps in human visual cortex. Neuroimage. 99:509–524.

Almeida J, Fintzi AR, Mahon BZ. 2013. Tool manipulation knowledge is retrieved by way of the ventral visual object processing pathway. Cortex. 49:2334–2344.

Amunts K, Schleicher A, Bürgel U, Mohlberg H, Uylings HB, Zilles K. 1999. Broca's region revisited: cytoarchitecture and intersubject variability. J Comp Neurol. 412:319–341.

Avanzini P, Abdollahi RO, Sartori I, Caruana F, Pelliccia V, Casaceli G, Mai R, Lo Russo G, Rizzolatti G, Orban GA. 2016. Four-dimensional maps of the human somatosensory system. Proc Natl Acad Sci USA. 113:E1936–E1943.

Bastin J, Lebranchu P, Jerbi K, Kahane P, Orban G, Lachaux J-P, Berthoz A. 2012. Direct recordings in human cortex reveal the dynamics of gamma-band [50–150 Hz] activity during pursuit eye movement control. Neuroimage. 63:339–347.

Beauchamp MS, Lee KE, Haxby JV, Martin A. 2002. Parallel visual motion processing streams for manipulable objects and human movements. Neuron. 34:149–159.

Blakemore S-J, Bristow D, Bird G, Frith C, Ward J. 2005. Somatosensory activations during the observation of touch and a case of vision-touch synaesthesia. Brain. 128:1571–1583.

Bouchard KE, Mesgarani N, Johnson K, Chang EF. 2013. Functional organization of human sensorimotor cortex for speech articulation. Nature. 495:327–332.

Brandi ML, Wohlschläger A, Sorg C, Hermsdörfer J, Wohlschlager A, Sorg C, Hermsdorfer J. 2014. The neural correlates of planning and executing actual tool use. J Neurosci. 34:13183–13194.

Buxbaum LJ. 2001. Ideomotor apraxia: a call to action. Neurocase. 7:445–458.

Buxbaum LJ, Giovannetti T, Libon D. 2000. The role of the dynamic body schema in praxis: evidence from primary progressive apraxia. Brain Cogn. 44:166–191.

Buxbaum LJ, Johnson-Frey SH, Bartlett-Williams M. 2005. Deficient internal models for planning hand–object interactions in apraxia. Neuropsychologia. 43:917–929.

Buxbaum LJ, Shapiro AD, Coslett HB. 2014. Critical brain regions for tool-related and imitative actions: a componential analysis. Brain. 137:1971–1985.

Cardinale F, Cossu M, Castana L, Casaceli G, Schiariti MP, Miserocchi A, Fuschillo D, Moscato A, Caborni C, Arnulfo G, et al. 2013. Stereoelectroencephalography: surgical methodology, safety, and stereotactic application accuracy in 500 procedures. Neurosurgery. 72:353–366. discussion 366.

Caruana F, Cantalupo G, Lo Russo G, Mai R, Sartori I, Avanzini P. 2014a. Human cortical activity evoked by gaze shift observation: an intracranial EEG study. Hum Brain Mapp. 35:1515–1528.

Caruana F, Sartori I, Lo Russo G, Avanzini P. 2014b. Sequencing biological and physical events affects specific frequency bands within the human premotor cortex: an intracerebral EEG study. PLoS ONE. 9:e86384.

Caruana F, Cuccio V. 2017. Types of abduction in tool behavior. Phenomenol Cogn Sci. 16:255–273.

Caspers S, Geyer S, Schleicher A, Mohlberg H, Amunts K, Zilles K. 2006. The human inferior parietal cortex: Cytoarchitectonic parcellation and interindividual variability. Neuroimage. 33: 430–448.

Caspers S, Zilles K, Laird AR, Eickhoff SB. 2010. ALE meta-analysis of action observation and imitation in the human brain. Neuroimage. 50:1148–1167.

Cattaneo L, Caruana F, Jezzini A, Rizzolatti G. 2009. Representation of Goal and Movements without Overt Motor Behavior in the Human Motor Cortex: A Transcranial Magnetic Stimulation Study. J Neurosci. 29:11134–11138.

Cattaneo L, Maule F, Barchiesi G, Rizzolatti G. 2013. The motor system resonates to the distal goal of observed actions: testing the inverse pliers paradigm in an ecological setting. Exp brain Res. 231:37–49.

Chan AW-Y, Baker CI. 2015. Seeing is not feeling: posterior parietal but not somatosensory cortex engagement during touch observation. J Neurosci. 35:1468–1480.

Chao LL, Haxby JV, Martin A. 1999. Attribute-based neural substrates in temporal cortex for perceiving and knowing about objects. Nat Neurosci. 2:913–919.

Chao LL, Martin A. 2000. Representation of manipulable man-made objects in the dorsal stream. Neuroimage. 12:478–484.

Chen Q, Garcea FE, Mahon BZ. 2016. The representation of object-directed action and function knowledge in the human brain. Cereb Cortex. 26:1609–1618.

Choi SH, Na DL, Kang E, Lee KM, Lee SW, Na DG. 2001. Functional magnetic resonance imaging during pantomiming tool-use gestures. Exp Brain Res. 139:311–317.

Dale AM, Fischl B, Sereno MI. 1999. Cortical surface-based analysis: I. Segmentation and surface reconstruction. Neuroimage. 9:179–194.

Davare M, Andres M, Cosnard G, Thonnard J-L, Olivier E. 2006. Dissociating the role of ventral and dorsal premotor cortex in precision grasping. J Neurosci. 26:2260–2268.

De Renzi E, Faglioni P 1999. Apraxia. In: Denes G and Pizzamiglio L, editor. Handbook of clinical and experimental neuropsychology. Hove: Psychology Press. p. 421–440.

Denys K, Vanduffel W, Fize D, Nelissen K, Peuskens H, Van Essen D, Orban GA. 2004. The processing of visual shape in the cerebral cortex of human and nonhuman primates: a functional magnetic resonance imaging study. J Neurosci. 24:2551–2565.

Disbrow EA, Slutsky DA, Roberts TP, Krubitzer LA. 2000a. Functional MRI at 1.5 tesla: a comparison of the blood oxygenation level-dependent signal and electrophysiology. Proc Natl Acad Sci USA. 97:9718–9723.

Disbrow E, Roberts T, Krubitzer L. 2000b. Somatotopic organization of cortical fields in the lateral sulcus of Homo sapiens: evidence for SII and PV. J Comp Neurol. 418:1–21.

Dumoulin SO, Bittar RG, Kabani NJ, Baker CL, Le Goualher G, Bruce Pike G, Evans AC. 2000. A new anatomical landmark for reliable identification of human area V5/MT: a quantitative analysis of sulcal patterning. Cereb Cortex. 10:454–463.

Eickhoff SB, Grefkes C, Zilles K, Fink GR. 2007. The somatotopic organization of cytoarchitectonic areas on the human parietal operculum. Cereb Cortex. 17:1800–1811.

Eklund A, Nichols TE, Knutsson H. 2016. Cluster failure: Why fMRI inferences for spatial extent have inflated false-positive rates. Proc Natl Acad Sci USA. 113:7900–7905.

Fang F, He S. 2005. Cortical responses to invisible objects in the human dorsal and ventral pathways. Nat Neurosci. 8: 1380–1385.

Ferri S, Rizzolatti G, Orban GA. 2015. The organization of the posterior parietal cortex devoted to upper limb actions: An fMRI study. Hum Brain Mapp. 36:3845–3866.

Gallese V, Fadiga L, Fogassi L, Rizzolatti G. 1996. Action recognition in the premotor cortex. Brain. 119:593–609.

Gallivan JP, Adam McLean D, Valyear KF, Culham JC. 2013. Decoding the neural mechanisms of human tool use. Elife. 2013:1–29.

Garcea FE, Dombovy M, Mahon BZ. 2013. Preserved tool knowledge in the context of impaired action knowledge: implications for models of semantic memory. Front Hum Neurosci. 7:120.

Garcea FE, Mahon BZ. 2014. Parcellation of left parietal tool representations by functional connectivity. Neuropsychologia. 60: 131–143.

Gering D, Nabavi A, Kikinis R, Grimson W, Hata N, Everett P, Jolesz F, Wells W. 1999. An integrated visualization system for surgical planning and guidance using image fusion and interventional imaging. In: Medical image computing and computer-assisted intervention – MICCAI'99. Berlin Heidelberg: Springer. p. 809–819.

Geyer S, Matelli M, Luppino G, Zilles K. 2000. Functional neuroanatomy of the primate isocortical motor system. Anat Embryol (Berl). 202:443–474.

Goldenberg G. 2009. Apraxia and the parietal lobes. Neuropsychologia. 47:1449–1459.

Goldenberg G, Hagmann S. 1998. Tool use and mechanical problem solving in apraxia. Neuropsychologia. 36:581–589.

Grafton ST, Fadiga L, Arbib MA, Rizzolatti G. 1997. Premotor cortex activation during observation and naming of familiar tools. Neuroimage. 236:231–236.

Grosbras M-H, Beaton S, Eickhoff SB. 2012. Brain regions involved in human movement perception: a quantitative voxel-based meta-analysis. Hum Brain Mapp. 33:431–454.

Heilman KM, Valenstein E. 2011. Clinical neuropsychology. New York: Oxford University Press.

Hihara S, Taoka M, Tanaka M, Iriki A. 2015. Visual responsiveness of neurons in the secondary somatosensory area and its surrounding parietal operculum regions in awake macaque monkeys. Cereb Cortex. 25:4535–4550.

Huk AC, Heeger DJ. 2002. Pattern-motion responses in human visual cortex. Nat Neurosci. 5:72–75.

Iriki A, Tanaka M, Iwamura Y. 1996. Coding of modified body schema during tool use by macaque postcentral neurones. Neuroreport. 7:2325–2330.

Ishida H, Fornia L, Grandi LC, Umiltà MA, Gallese V. 2013. Somato-motor haptic processing in posterior inner perisylvian region (SII/pIC) of the macaque monkey. PLoS ONE. 8: e69931.

Jastorff J, Abdollahi RO, Orban GA. 2012. Acting alters visual processing: flexible recruitment of visual areas by one's own actions. Cereb Cortex. 22:2930–2942.

Johansson RS, Flanagan JR. 2009. Coding and use of tactile signals from the fingertips in object manipulation tasks. Nat Rev Neurosci. 10:345–359.

Johansson RS, Westling G, Bäckström A, Flanagan JR. 2001. Eye-hand coordination in object manipulation. J Neurosci. 21: 6917–6932.

Johnson-Frey SH. 2004. The neural bases of complex tool use in humans. Trends Cogn Sci. 8:71–78.

Johnson-Frey SH, Newman-Norlund R, Grafton ST. 2005. A distributed left hemisphere network active during planning of everyday tool use skills. Cereb Cortex. 15:681–695.

Kadipasaoglu CM, Baboyan VG, Conner CR, Chen G, Saad ZS, Tandon N. 2014. Surface-based mixed effects multilevel analysis of grouped human electrocorticography. Neuroimage. 101:215–224.

Kellenbach ML, Brett M, Patterson K. 2003. Actions speak louder than functions: the importance of manipulability and action in tool representation. J Cogn Neurosci. 15:30–46.

Kersey AJ, Clark TS, Lussier CA, Mahon BZ, Cantlon JF. 2016. Development of tool representations in the dorsal and ventral visual object processing pathways. Cereb Cortex. 26: 3135–3145.

Keysers C, Wicker B, Gazzola V, Anton J-L, Fogassi L, Gallese V. 2004. A touching sight: SII/PV activation during the observation and experience of touch. Neuron. 42:335–346.

Kolster H, Peeters R, Orban GA. 2010. The retinotopic organization of the human middle temporal area MT/V5 and its cortical neighbors. J Neurosci. 30:9801–9820.

Kourtzi Z, Kanwisher N. 2001. Representation of perceived object shape by the human lateral occipital complex. Science. 293:1506–1509.

Kraskov A, Philipp R, Waldert S, Vigneswaran G, Quallo MM, Lemon RN. 2014. Corticospinal mirror neurons. Philos Trans R Soc Lond B Biol Sci. 369:20130174.

Króliczak G, Frey SH. 2009. A common network in the left cerebral hemisphere represents planning of tool use pantomimes and familiar intransitive gestures at the hand-independent level. Cereb Cortex. 19:2396–2410.

Lachaux J-P, Axmacher N, Mormann F, Halgren E, Crone NE, Lyon CB. 2012. High-frequency neural activity and human cognition: past, present and possible future of intracranial EEG research. Prog Neurobiol. 98:279–301.

Lagae L, Maes H, Raiguel S, Xiao DK, Orban GA. 1994. Responses of macaque STS neurons to optic flow components: a comparison of areas MT and MST. J Neurophysiol. 71:1597–1626.

Lewis JW. 2006. Cortical networks related to human use of tools. Neuroscientist. 12:211–231.

Logothetis NK. 2008. What we can do and what we cannot do with fMRI. Nature. 453:869–878.

Mahon BZ, Kumar N, Almeida J. 2013. Spatial frequency tuning reveals interactions between the dorsal and ventral visual systems. J Cogn Neurosci. 25:862–871.

Mahon BZ, Milleville SC, Negri GAL, Rumiati RI, Caramazza A, Martin A. 2007. Action-related properties shape object representations in the ventral stream. Neuron. 55:507–520.

Manning JR, Jacobs J, Fried I, Kahana MJ. 2009. Broadband shifts in local field potential power spectra are correlated with single-neuron spiking in humans. J Neurosci. 29: 13613–13620.

Maravita A, Iriki A. 2004. Tools for the body (schema). Trends Cogn Sci. 8:79–86.

Martin A, Wiggs CL, Ungerleider LG, Haxby JV. 1996. Neural correlates of category-specific knowledge. Nature. 379:649–652.

Méndez-Bértolo C, Moratti S, Toledano R, Lopez-Sosa F, Martínez-Alvarez R, Mah YH, Vuilleumier P, Gil-Nagel A, Strange BA. 2016. A fast pathway for fear in human amygdala. Nat Neurosci. 19:1041–1049.

Molenberghs P, Cunnington R, Mattingley JB. 2012. Brain regions with mirror properties: A meta-analysis of 125 human fMRI studies. Neurosci Biobehav Rev. 36:341–349.

Moll J, de Oliveira-Souza R, Passman LJ, Cunha FC, Souza-Lima F, Andreiuolo PA. 2000. Functional MRI correlates of real and imagined tool-use pantomimes. Neurology. 54:1331–1336.

Mruczek REB, von Loga IS, Kastner S. 2013. The representation of tool and non-tool object information in the human intraparietal sulcus. J Neurophysiol. 109:2883–2896.

Murata A, Fadiga L, Fogassi L, Gallese V, Raos V, Rizzolatti G. 1997. Object representation in the ventral premotor cortex (area F5) of the monkey. J Neurophysiol. 78:2226–2230.

Nelissen K, Vanduffel W, Orban GA. 2006. Charting the lower superior temporal region, a new motion-sensitive region in monkey superior temporal sulcus. J Neurosci. 26:5929–5947.

Noppeney U, Price CJ, Penny WD, Friston KJ. 2006. Two distinct neural mechanisms for category-selective responses. Cereb Cortex. 16:437–445.

Ochipa C, Rothi LJ, Heilman KM. 1989. Ideational apraxia: a deficit in tool selection and use. Ann Neurol. 25:190–193.

Orban GA, Caruana F. 2014. The neural basis of human tool use. Front Psych. 5:310.

Osiurak F, Badets A. 2016. Tool use and affordance: Manipulation-based versus reasoning-based approaches. Psychol Rev. 123: 534–568.

Osiurak F, Jarry C, Allain P, Aubin G, Etcharry-Bouyx F, Richard I, Bernard I, Le Gall D. 2009. Unusual use of objects after unilateral brain damage. The technical reasoning model. Cortex. 45:769–783.

Osiurak F, Jarry C, Le Gall D. 2010. Grasping the affordances , understanding the reasoning : toward a dialectical theory of human tool use franc. Psychol Rev. 117:517–540.

Parvizi J, Jacques C, Foster BL, Witthoft N, Withoft N, Rangarajan V, Weiner KS, Grill-Spector K. 2012. Electrical stimulation of human fusiform face-selective regions distorts face perception. J Neurosci. 32:14915–14920.

Peeters R, Simone L, Nelissen K, Fabbri-Destro M, Vanduffel W, Rizzolatti G, Orban GA. 2009. The representation of tool use in humans and monkeys: common and uniquely human features. J Neurosci. 29:11523–11539.

Peeters RR, Rizzolatti G, Orban GA. 2013. Functional properties of the left parietal tool use region. Neuroimage. 78:83–93.

Ray S, Maunsell JHR. 2011. Different origins of gamma rhythm and high-gamma activity in macaque visual cortex. PLoS Biol. 9:e1000610.

Reynaud E, Lesourd M, Navarro J, Osiurak F. 2016. On the neurocognitive origins of human tool use: a critical review of neuroimaging data. Neurosci Biobehav Rev. 64:421–437.

Rizzolatti G, Cattaneo L, Fabbri-Destro M, Rozzi S. 2014. Cortical mechanisms underlying the organization of goal-directed actions and mirror neuron-based action understanding. Physiol Rev. 94:655–706.

Rizzolatti G, Fadiga L, Gallese V, Fogassi L. 1996. Premotor cortex and the recognition of motor actions. Brain Res Cogn Brain Res. 3:131–141.

Rizzolatti G, Fogassi L, Gallese V. 2001. Neurophysiological mechanisms underlying the understanding and imitation of action. Nat Rev Neurosci. 2:661–670.

Rochat MJ, Caruana F, Jezzini A, Escola L, Intskirveli I, Grammont F, Gallese V, Rizzolatti G, Umiltà MA. 2010. Responses of mirror neurons in area F5 to hand and tool grasping observation. Exp brain Res. 204:605–616.

Rothi LJ, Heilman KM, Watson RT. 1985. Pantomime comprehension and ideomotor apraxia. J Neurol Neurosurg Psychiatry. 48:207–210.

Rumiati RI, Weiss PH, Shallice T, Ottoboni G, Noth J, Zilles K, Fink GR. 2004. Neural basis of pantomiming the use of visually presented objects. Neuroimage. 21:1224–1231.

Rumiati RI, Zanini S, Vorano L, Shallice T. 2001. A form of ideational apraxia as a delective deficit of contention scheduling. Cogn Neuropsychol. 18:617–642.

Sawamura H, Orban GA, Vogels R. 2006. Selectivity of neuronal adaptation does not match response selectivity: a single-cell study of the fMRI adaptation paradigm. Neuron. 49: 307–318.

Scheperjans F, Eickhoff SB, Hömke L, Mohlberg H, Hermann K, Amunts K, Zilles K. 2008. Probabilistic maps, morphometry, and variability of cytoarchitectonic areas in the human superior parietal cortex. Cereb Cortex. 18:2141–2157.

Umiltà MA, Escola L, Intskirveli I, Grammont F, Rochat M, Caruana F, Jezzini A, Gallese V, Rizzolatti G. 2008. When pliers become fingers in the monkey motor system. PNAS. 105: 2209–2213.

Valyear KF, Cavina-Pratesi C, Stiglick AJ, Culham JC. 2007. Does tool-related fMRI activity within the intraparietal sulcus reflect the plan to grasp? Neuroimage. 36(Suppl 2):T94–T108.

Valyear KF, Gallivan JP, Mclean DA, Culham JC. 2012. fMRI repetition suppression for familiar but not arbitrary actions with tools. J Neurosci. 32:4247–4259.

Vigneswaran G, Philipp R, Lemon RN, Kraskov A. 2013. M1 corticospinal mirror neurons and their role in movement suppression during action observation. Curr Biol. 23:236–243.

Vingerhoets G. 2008. Knowing about tools: neural correlates of tool familiarity and experience. Neuroimage. 40:1380–1391.

Vingerhoets G, Vandamme K, Vercammen A. 2009. Conceptual and physical object qualities contribute differently to motor affordances. Brain Cogn. 69:481–489.

Zeki S, Watson JD, Lueck CJ, Friston KJ, Kennard C, Frackowiak RS. 1991. A direct demonstration of functional specialization in human visual cortex. J Neurosci. 11:641–649.